Analysis and simulation of chemical explosions in nonspherical cavities in granite

Jeffry L. Stevens,[1] Steven Gibbons,[2] Norton Rimer,[1] Heming Xu,[1] Conrad Lindholm,[2] Frode Ringdal,[2] Tormod Kvaerna,[2] and John R. Murphy[1]

Received 6 April 2005; revised 26 October 2005; accepted 18 January 2006; published 25 April 2006.

[1] We analyze data from 15 decoupled chemical explosions conducted from 1986 to 2002 in Älvdalen, Sweden, recorded on regional seismic stations NORES, HFS, and NORSAR. The explosions were conducted in three approximately rectangular granite chambers at a depth of 100 m in chambers with volumes of 200, 300, and 1000 m^3 and yields ranging from 500 to 10,000 kg. The smallest explosions in the largest chamber are fully decoupled, while the other explosions are partially coupled, overdriven by up to a factor of 25. The data show that decoupling remains fairly constant for overdrive up to about a factor of 10 then decreases rapidly at higher yields. Several 1000 kg explosions were conducted in the two smaller chambers. These events did not appear in seismic bulletins; however, we were able to identify the waveform and to estimate the origin time using a waveform correlation procedure. For the more recent explosions, near-field data were recorded on pressure gauges in the chamber and adjacent tunnel and on velocity gauges in boreholes at several locations near the chamber. We have modeled these data using three-dimensional finite difference calculations. The calculations show enhanced signals in the direction along the small axis of the chamber and reduced signals near the long end of the tunnel. Although we do not have free-field data from all directions, the data for the available locations are consistent with these calculations.

Citation: Stevens, J. L., S. Gibbons, N. Rimer, H. Xu, C. Lindholm, F. Ringdal, T. Kvaerna, and J. R. Murphy (2006), Analysis and simulation of chemical explosions in nonspherical cavities in granite, *J. Geophys. Res.*, *111*, B04306, doi:10.1029/2005JB003768.

1. Introduction

[2] It is well known that the seismic signals from an explosion can be reduced (decoupled) by detonating the explosion in a large chamber [*Herbst et al.*, 1961]. The physical mechanisms for the generation of seismic signals from fully decoupled explosions are relatively simple and well understood, corresponding to shock and reverberations from pressurized gas within a linear elastic medium [*Stevens et al.*, 1991]. The seismic signals from tamped explosions are more complex but are constrained by a large volume of data. However, the partially coupled case, where the explosion yield relative to the cavity size is too large to be fully decoupled but smaller than fully tamped, is less well understood and constrained by only a small volume of data. In addition, there is substantial uncertainty regarding the effect of nonspherical cavities on decoupling effectiveness. This is important because nonspherical cavities are less expensive and easier to construct than spherical cavities of equivalent volume. *Murphy et al.* [1997] studied a series of 12 decoupled HE explosions in mined spherical and cylindrical cavities in hard limestone in Kyrgyzstan. They concluded that low-frequency decoupling factors were insensitive to cavity shape, and found a maximum observed decoupling factor of 25 for this data set. In this paper we describe experiments using partially coupled chemical explosions in approximately rectangular granite chambers that place some additional constraints on the seismic coupling from such events.

[3] Fifteen decoupled chemical explosions were conducted from 1986 to 2002 in Älvdalen, Sweden (Figure 1). The cavity explosions, which comprise two separate series of experiments (1986–1996 and 2000–2002) are listed in Table 1. Descriptions of these experiments are provided by *Grønsten* [2000], *Grønsten and Krest* [2002], *Forsén et al.* [1997], *Hansson and Forsén* [1997], and *Vretblad* [1991]. All but two of the explosions were recorded by the NORES and NORSAR arrays. The last explosion occurred shortly after NORES was damaged by lightning. The last six were also recorded on the HFS array in Sweden. NORSAR participated in the explosions during the summer of 2001 and 2002. They deployed a number of temporary instruments including one surface instrument for each event on site near the explosion. The last five explosions were conducted in a cavity approximately 4 m high by 8 m wide by 30 m long (1000 m^3). The first 10 explosions were in two smaller chambers approximately 3 m high by 4 m wide with lengths of 17 m (200 m^3) and 25 m (300 m^3). Explosive yields ranged from 500 to 10,000 kg, with charges consisting of TNT, ANFO, and ammunition shells. The smallest two

[1] Science Applications International Corporation, San Diego, California, USA.
[2] NORSAR, Kjeller, Norway.

0148-0227/06/2005JB003768$09.00

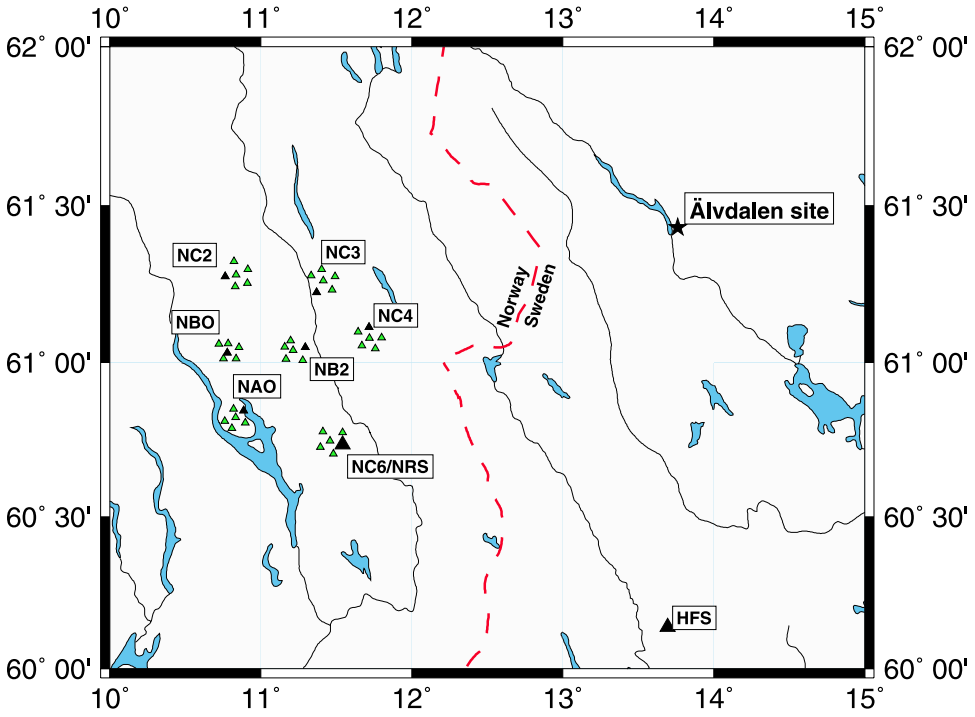

Figure 1. Location of the explosion site relative to the HFS and NORES (NRS) arrays and the seven NORSAR subarrays. The dashed line is the Norway/Sweden national boundary.

explosions in the largest chamber appear to be fully decoupled, while the other explosions are partially coupled. Near-field data were recorded on pressure gauges in the chamber and adjacent tunnel, and on velocity gauges in boreholes at several locations near the chamber. The entrance to the chamber is open, so the blast wave from the chamber explosion propagates out of the chamber and down the adjacent tunnel. Since the open tunnel depressurizes the chamber, analysis based on a closed chamber is only valid up to a time corresponding to the characteristic decay time associated with venting of cavity pressure down the tunnel. Pressure measurements in the adjacent tunnel take about 3 s to decay to half of the peak value. This time is much longer than the time used for near-field data analysis and modeling.

2. Decoupling Theory and Criteria for Full Decoupling

[4] A simplified source function for a fully decoupled explosion can be described as a pressure pulse applied to the wall of a cavity in an elastic medium. The actual physics is more complicated than this: there are reverberations in the cavity that cause high-frequency spectral peaks, and the shock wave that hits the wall is stronger than an instantaneously applied pressure pulse corresponding to a uniformly

Table 1. Cavity Decoupled Explosions at the Älvdalen Site[a]

Origin ID	Explosion Origin Time, year-day:LT	Explosion Charge, kg	Explosive	Chamber Volume,[b] m^3	Charge/Volume, kg/m^3
1986C168	1986-168:1006.15.9	1000	TNT	300	3.3
1986C177	1986-177:0914.06.6	1000	TNT	200	5.0
1986C246	1986-246:1150.45.1	1000	Shells (TNT)	200	5.0
1986C260	1986-260:1134.17.4	1000	Shells (TNT)	300	3.3
1987C141	1987-141:1016.08.3	1000	ANFO	300	3.3
1987C146	1987-146:1047.38.2	5000	ANFO[c]	300	16.7
1987C259	1987-259:1036.13.0	5000	ANFO	200	25.0
1989C242	1989-242:1012.21.0	1000	Shells (TNT)	300	3.3
1989C263	1989-263:1006.03.5	5000	ANFO	300	16.7
1996C269	1996-269:1100.13.9	1000	Shells (TNT)	300	3.3
2000C343	2000-343:1043.04.5	500	TNT	1000	0.5
2000C348	2000-348:1003.02.0	10000	TNT	1000	10
2001C150	2001-150:1003.56.2	2500	TNT	1000	2.5
2001C186	2001-186:1041.23.5	10000	Shells (TNT)	1000	10
2002C164	2002-164:0859.25.1	10000	TNT/powder	1000	10

[a]Origin times of the last four 2000–2002 events were determined from a station at the explosion site. Origin times of earlier events were determined by waveform correlation with the later events.
[b]Chamber volume excludes access tunnel.
[c]The ANFO explosive used in the 1987 and 1989 events had an explosion equivalent of 0.82 of TNT.

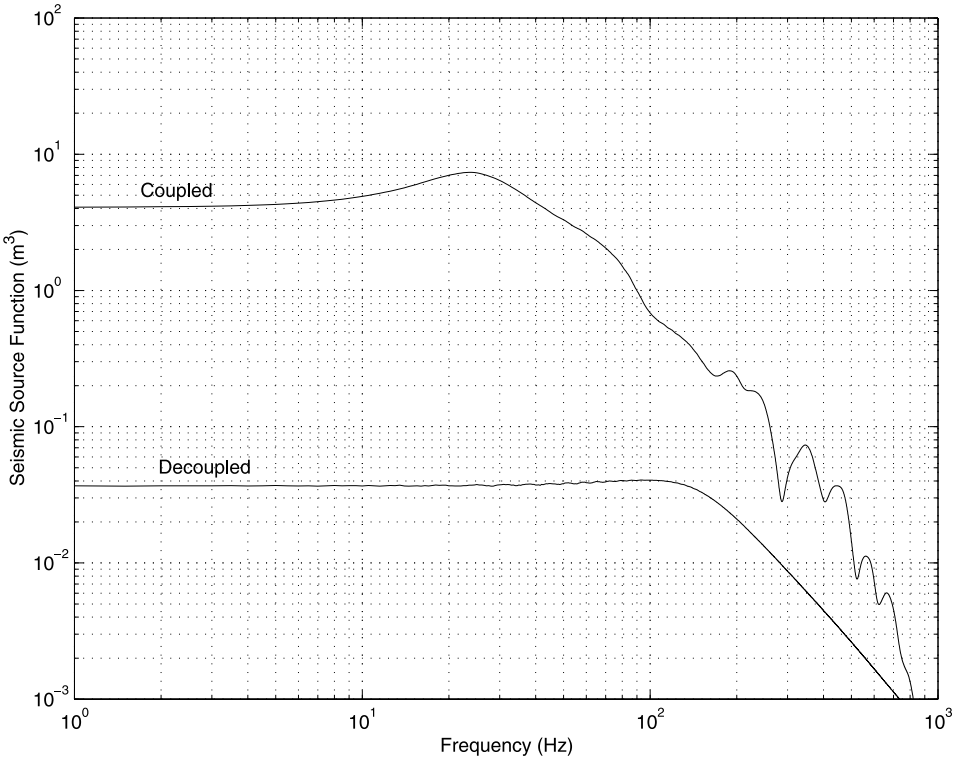

Figure 2. Source functions (RVP) for fully coupled and fully decoupled 10 t chemical explosions. The calculations are for chemical explosions in granite at a depth of 100 m. The decoupled explosion is modeled as a step pressure source in a spherical cavity with a volume of 1000 m^3.

pressurized cavity [e.g., *Stevens et al.*, 1991]. However, the simple model is useful for illustration and has many of the characteristics of a decoupled explosion. This description is also applicable to nonspherical cavities; however, nonspherical cavities will become partially coupled at smaller yields because the smallest cavity dimension is closer to the source and will be impacted by a stronger shock wave than the spherical cavity.

[5] The reduced velocity potential (RVP) for a pressure pulse $P(t)$ with derivative $\dot{P}(t)$ and corresponding Fourier transforms $P(\omega)$ and $\dot{P}(\omega)$ applied to the wall of a spherical cavity is

$$\dot{\psi}(\omega) = \dot{P}(\omega)\frac{R^3\omega_0^2}{4\mu}\frac{e^{i\omega/\omega_0}}{\omega_0^2 + i\omega\omega_0 - [(\lambda+2\mu)/4\mu]\omega^2} \quad (1)$$

where $\omega_0 = \alpha/R$, where R is the cavity radius, α is the compressional velocity of the external medium, and λ and μ are the Lame constants of the external medium. For a step in pressure of magnitude P_0 applied at time $t = 0$, $\dot{P}(\omega) = P_0$, and for this or any pressure pulse with static value P_0, in the low-frequency limit, we have

$$\psi_\infty = P_0R^3/4\mu \quad (2)$$

For an explosion in an air-filled cavity, the static value of the pressure is related to the yield W by

$$P_0 = \frac{(\gamma-1)W}{V} \quad (3)$$

where γ is the adiabatic expansion constant, which is approximately 1.2 for strong shocks in air and 1.3 for chemical explosion products, and V is the cavity volume. In SI units, W is in joules and 1 kt is equivalent to 4.2×10^{12} J.

[6] The "decoupling factor" D is defined as the ratio of the fully coupled to decoupled source:

$$D = \psi_{\text{tamped}}/\psi_{\text{decoupled}} \quad (4)$$

Figure 2 shows the coupled and decoupled source function and Figure 3 shows the frequency-dependent decoupling factor obtained by taking the ratio of coupled to decoupled source for a 10 t chemical explosion in granite at a depth of 100 m. The decoupled source function was calculated using the analytic solution for a pressurized sphere (equation (1)), while the coupled source function was calculated using a spherically symmetric finite difference calculation as described in section 5.3. The theoretical decoupling factor decreases with frequency, declining by an order of magnitude at frequencies above 25 Hz.

[7] The approximate criterion for full decoupling is usually expressed in terms of a requirement that the late time, equilibrium pressure in the cavity be less than or equal to some constant, k, times the overburden pressure [*Herbst et al.*, 1961]:

$$\frac{(\gamma-1)W}{V} \le k\rho gh \quad (5)$$

where k is between 0.5 (Latter) and 1.0 (Patterson), and ρgh is the overburden pressure at depth h.

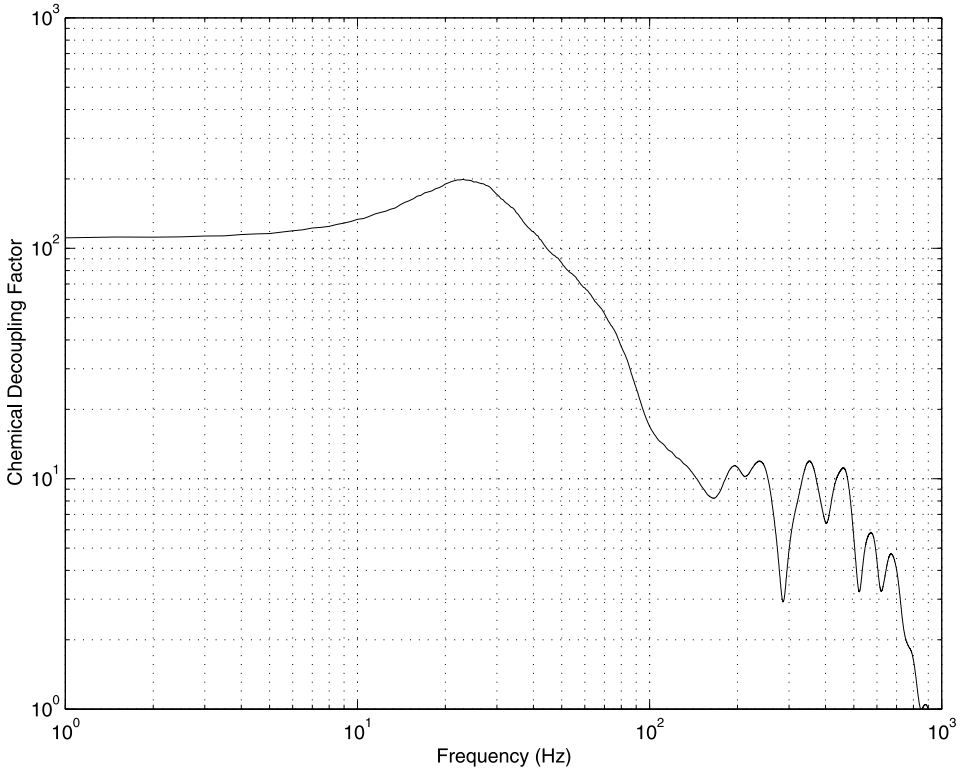

Figure 3. Frequency-dependent decoupling factor for the RVPs shown in Figure 2.

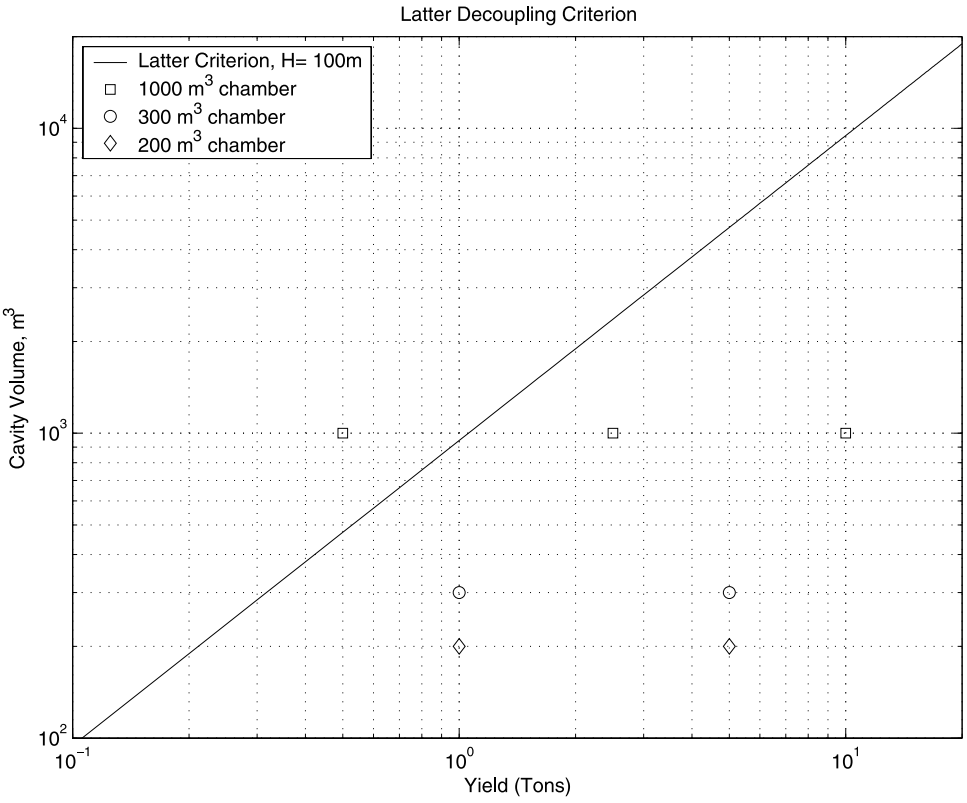

Figure 4. Latter decoupling criterion calculated for the conditions of the Swedish chamber explosions. The actual values for the Swedish chamber explosions are marked.

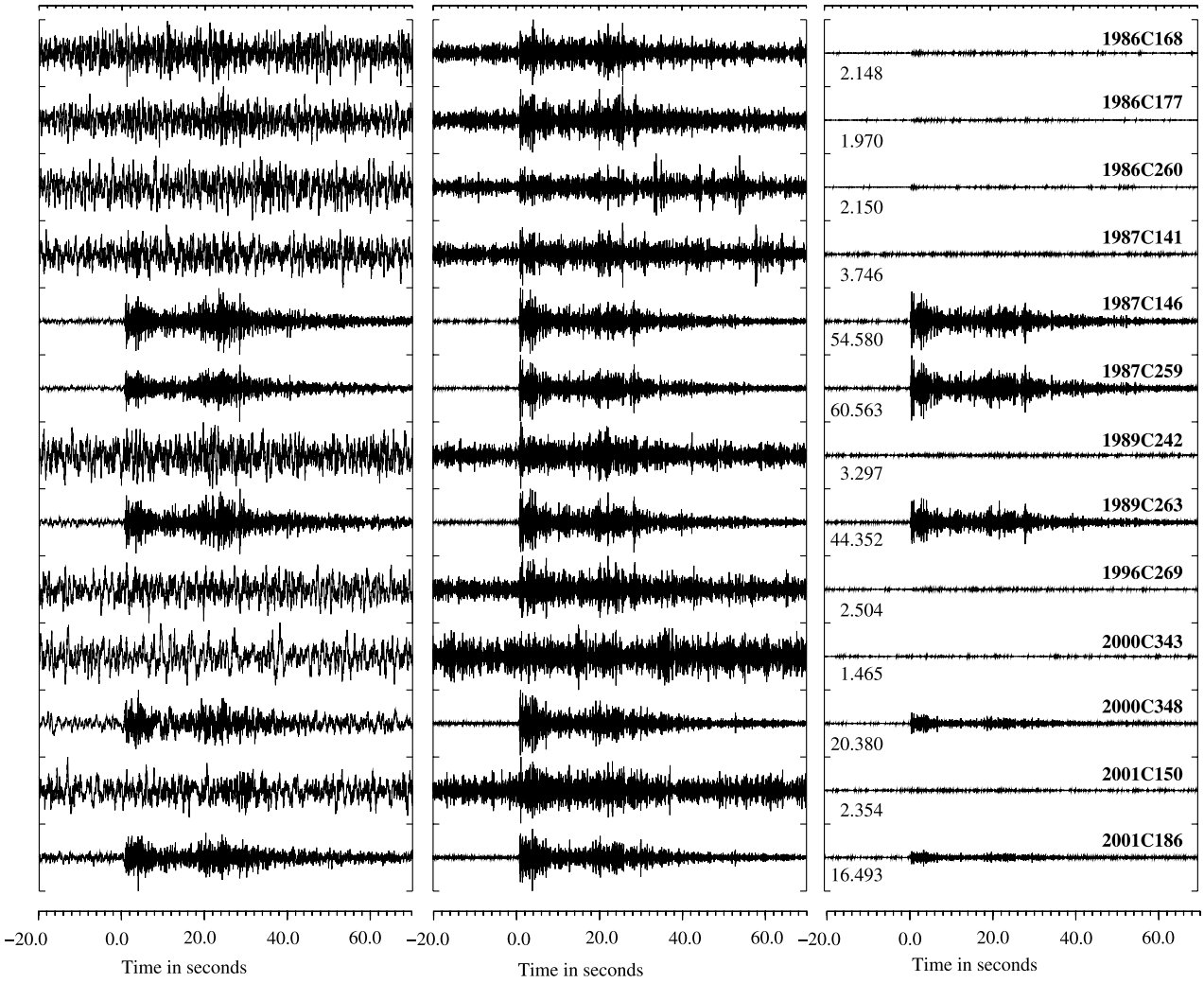

Figure 5. Waveforms from the NORES central element NRA0 (vertical component) for all of the Älvdalen explosions listed in Table 1 (except for events 1986C246 and 2002C164 for which NORES data do not exist). Waveforms are unfiltered in Figure 5 (left) and filtered between 8.0 and 16.0 Hz in Figure 5 (middle). The filtered waveforms are displayed in Figure 5 (right) to a common vertical scale. Only the events with charge loading density greater than 10 kg/m^3 are visible without filtering, the events with charge density between 2.5 and 5.0 kg/m^3 are detectable using standard array processing when band-pass filtered at high frequencies, and the signal from the 2000C343 event (charge density = 0.5 kg/m^3) is essentially indistinguishable from the noise even with filtering.

[8] The Swedish chamber explosions are at 100 m depth in granite. Figure 4 shows the Latter criterion for full decoupling together with the actual parameters calculated from the known depth and volume for each of these explosions. All but one of the explosions exceeds the Latter threshold. The 2500 kg explosion in the 1000 m^3 chamber is also close to fully decoupled. Note that the charge per volume listed in Table 1 is approximately equal to the amount of overdrive above full decoupling according to the Latter criterion.

3. Regional Data for Decoupled Chamber Explosions

[9] Figure 5 shows unfiltered and filtered waveforms for 13 of the underground explosions in Älvdalen recorded at NORES (the other two events were not recorded at NORES). The signals resulting from three events from 1987 and 1989, which were 5000 kg explosions in 200 m^3 and 300 m^3 chambers, have much larger amplitudes than the 10,000 kg events which were in the larger 1000 m^3 chamber in 2000 and 2001. The signal from the 2500 kg explosion in the 1000 m^3 chamber is indistinguishable from the noise without filtering of the data.

[10] In order to quantify the differences between these events, we examine the spectra in three time windows. For each component, time windows were defined corresponding to the P arrival, S arrival, and preevent noise (Figure 6). A 5 s window of waveform data was extracted immediately after the P onset, and a 10 s window immediately after the S onset. A 10 s window

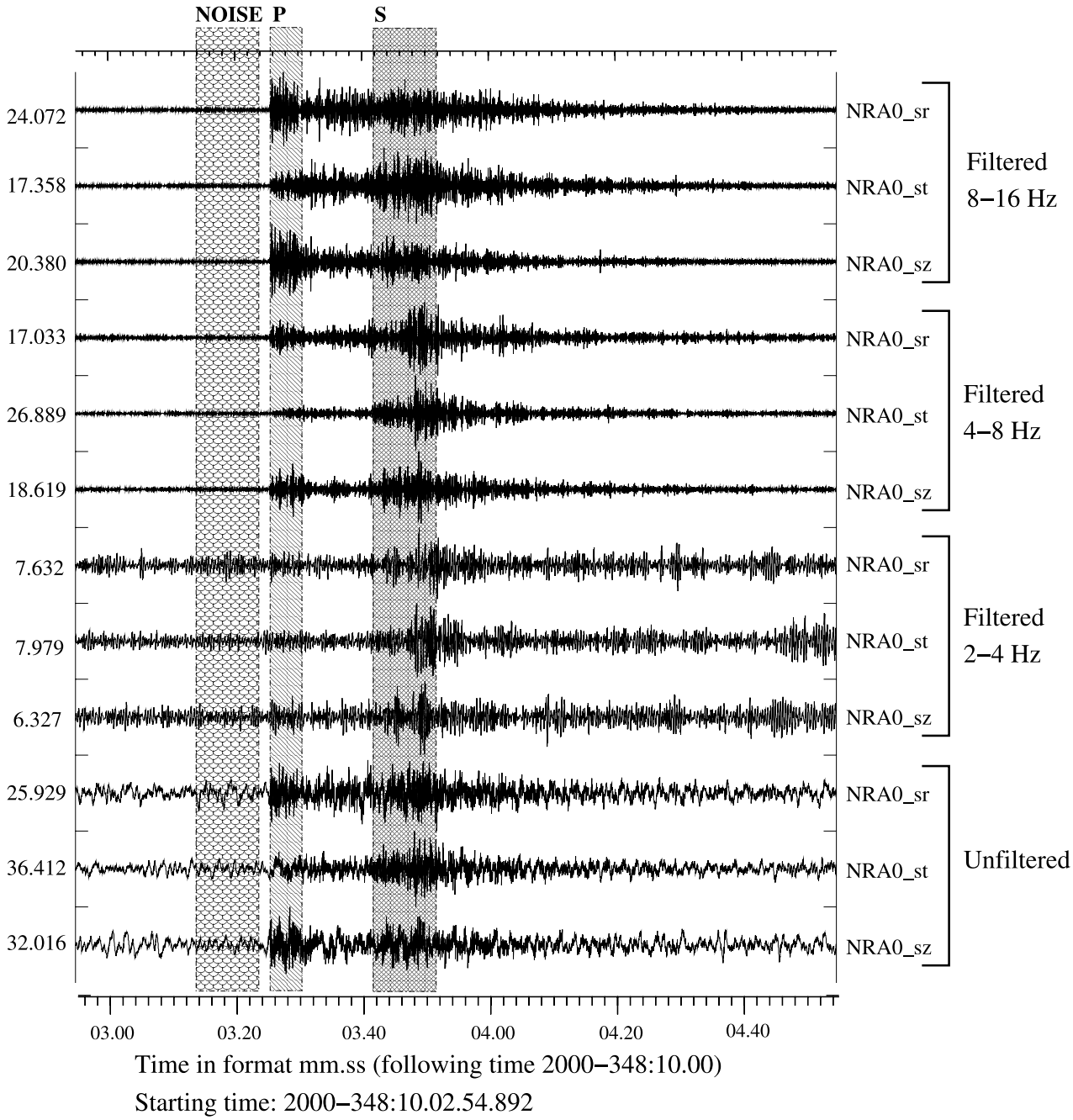

Figure 6. Waveform data for event 2000C348 as recorded by the NORES central instrument, NRA0. The horizontal components are rotated toward the source with a back azimuth of 56°. The lowermost three traces are unfiltered data, and the remaining traces are filtered with a Butterworth band-pass filter in the frequency bands 2.0–4.0 Hz, 4.0–8.0 Hz, and 8.0–16.0 Hz as indicated. Each group of three traces contains the vertical component (z) and the rotated radial (r) and transverse (t) traces. The time windows used to calculate spectra are marked.

ending 2 s before the P onset was defined in order to quantify the level of noise which is expected in the signal.

[11] Amplitude spectral density was calculated for each time window, with the instrument removed to correct to velocity. The amplitude spectral density was calculated by taking the square root of the power spectral density. Amplitude spectral density, averaged over the vertical components of the NORES array are shown in Figure 7 for the 12 explosions listed in Table 1 that had measurable NORES data, for frequencies up to the Nyquist frequency of 20 Hz. The results shown in Figure 7 clearly show the effect of substantially greater decoupling for the larger chamber relative to the smaller chamber.

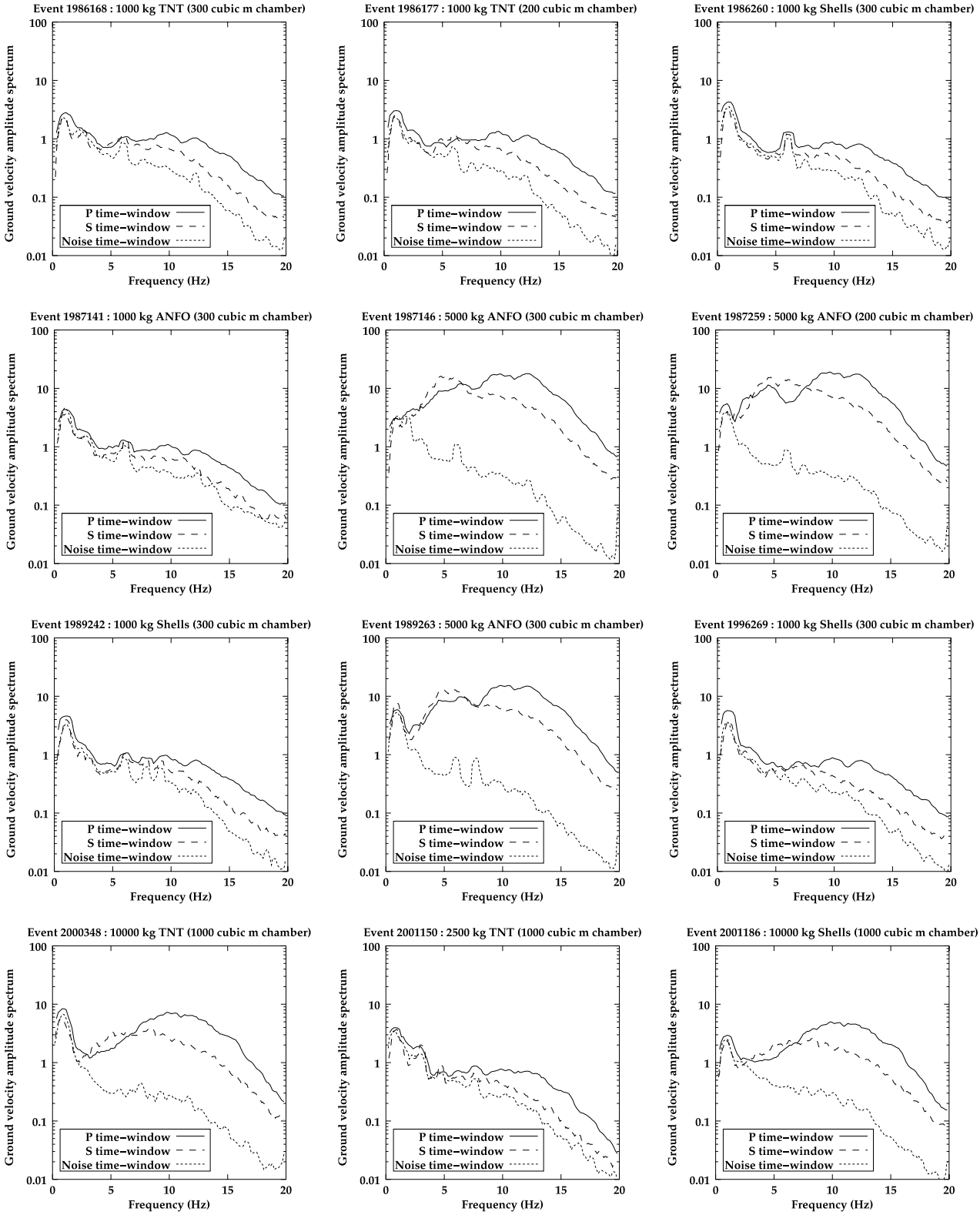

Figure 7. Average amplitude spectral density from NORES vertical component data for the 12 decoupled explosions as indicated; all instrument corrected to velocity. The solid line corresponds to the P window, the dashed line corresponds to the S window, and the dotted black line corresponds to the noise window.

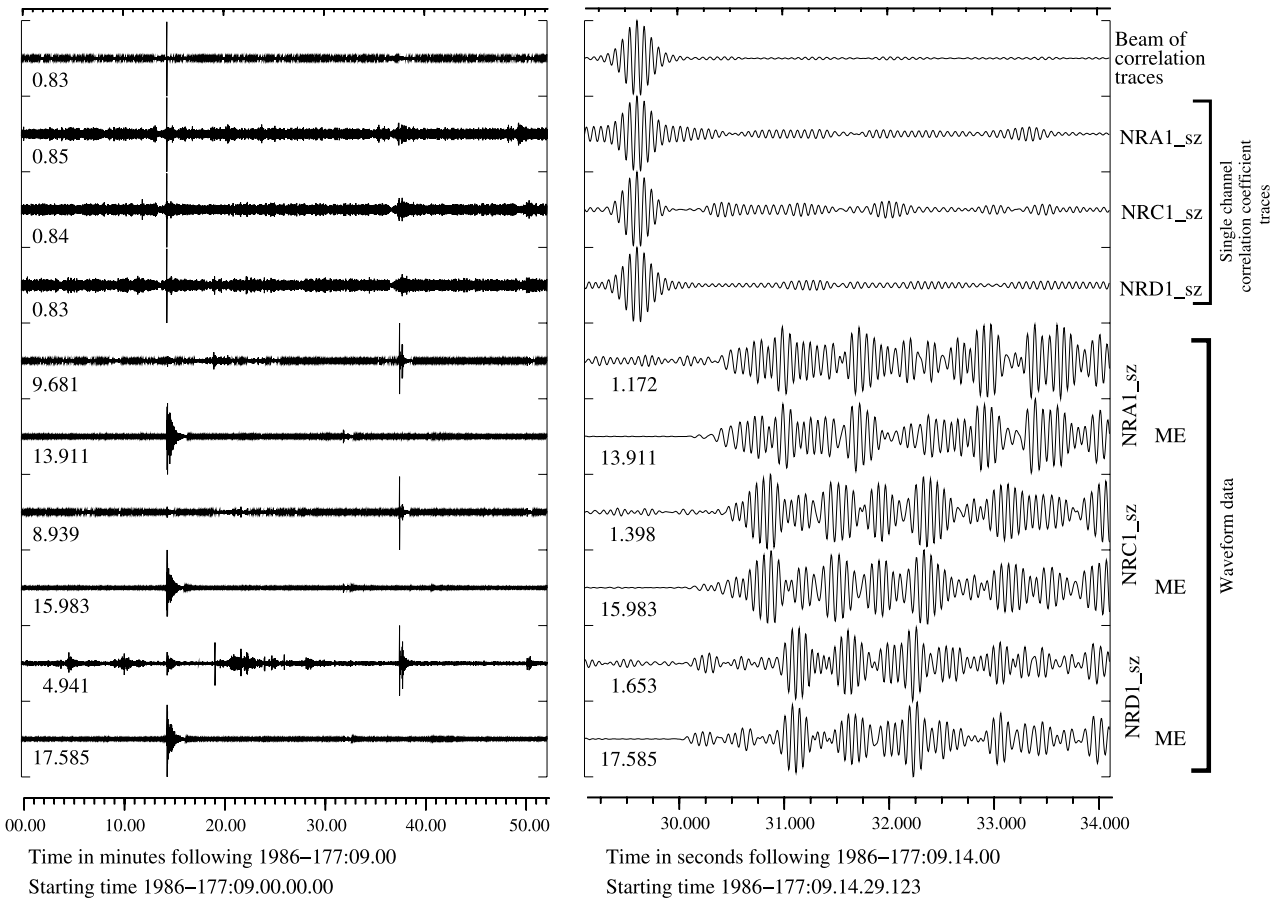

Figure 8. Detection of Älvdalen event 1986C177 using NORES data and waveform correlation with the 1987C259 event signal as a master event (ME). A template of length 60.0 s was taken from the 1987 event beginning with the P phase arrival. Waveforms are band-pass filtered between 14 and 18 Hz. Note the high correlation coefficient in spite of the high frequencies used and in spite of the fact that these two events took place in different chambers. Data from the master event aligned with the 1986 data according to the maximum correlation coefficient are shown. The amplitude of the master event signal is over 10 times that for the 1986 event.

[12] The 500 kg and seven 1000 kg events did not appear in any seismic bulletin and a visual search of the records for the corresponding day (the time was not available) identified only one probable signal. We therefore developed a waveform correlation technique using the event with the largest signal (1987C259) as a master event. The data from this event were cross-correlated with the data for the known day of each event. Arrivals from all six of the 1000 kg events and the 500 kg event were identified using this technique. Figure 8 shows an example for event 1986C177.

[13] Figure 9 shows NORES amplitude spectra for all events for which NORES data exists and is measurable in the 10–20 Hz frequency band. Each line in Figure 9 is the arithmetic mean of a spectrum calculated using the Thomson multitaper method [*Thomson*, 1982] from each of the available NORES short-period channels in an 8.0 s time window beginning at the first P arrival. Spectra are corrected to velocity.

[14] Figure 10 shows the mean P wave spectral amplitude averaged between 10 and 15 Hz, scaled by yield and plotted against the charge density in the chamber. Figure 10 shows a clear increase in coupling with charge density for explosions in the same chamber. However, for the same change density, the larger chamber appears to decouple substantially better than the smaller chambers.

4. Near-Field Recordings From the Decoupled Explosions

[15] Near-field accelerometer recordings were made available by the Norwegian Defense Building and Infrastructure Agency (Forsvarsbygg) for the decoupled explosions in 2000 and 2001 (2000C348, 2001C150 and 2001C186 in Table 1), with additional pressure measurements from within the detonation chamber for the two decoupled explosions in 2001. All of these tests were conducted in the $4 \times 8 \times 30$ m (1000 m^3) chamber. The acceleration data consists of three-component recordings in vertical boreholes and two two-component (vertical plus parallel to long axis of chamber) at soil and rock sites. The boreholes are located at distances of 11, 22.6,

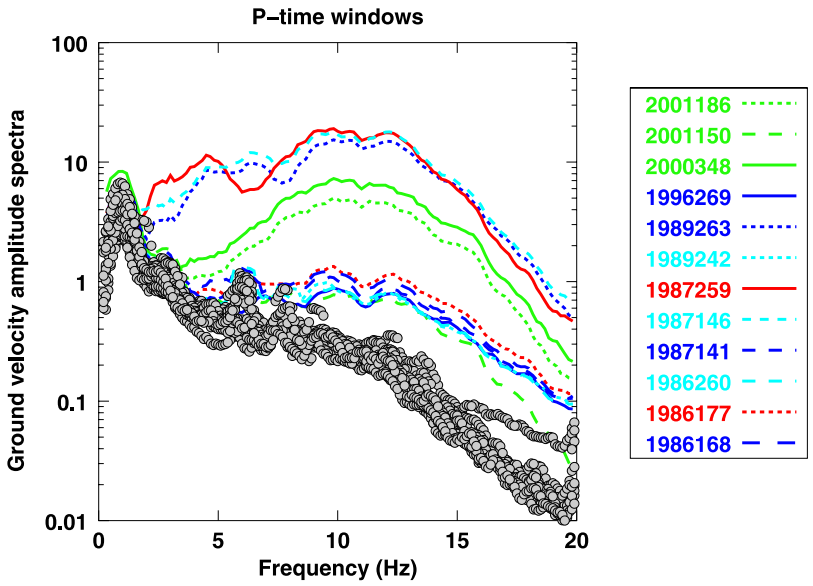

Figure 9. Amplitude spectra from the Älvdalen explosions for which NORES data exist. Green lines are for events which took place in the 1000 m^3 chamber, blue lines are for events which took place in chamber A (300 m^3), and red lines are for events which took place in chamber B (200 m^3). Circles show noise measurements for all events.

and 45.2 m west of the chamber wall, while the surface accelerometers have an assumed location 96.5 m west (assumed along the same line) of the chamber wall. The accelerometer locations relative to the detonation chamber are shown in Figure 11. Since we are primarily interested in the decoupled explosion source function rather than the effects of local structure, only the borehole data was used in the following modeling study. *Wu et al.* [2003] used the

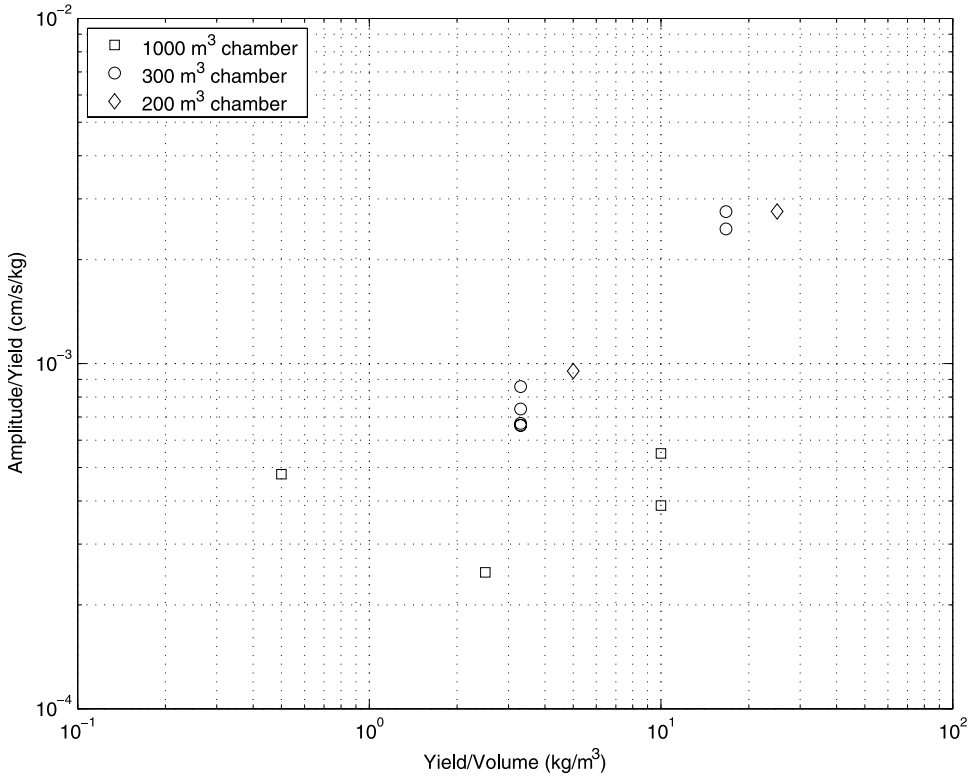

Figure 10. Yield scaled amplitude plotted versus charge density (yield divided by chamber volume).

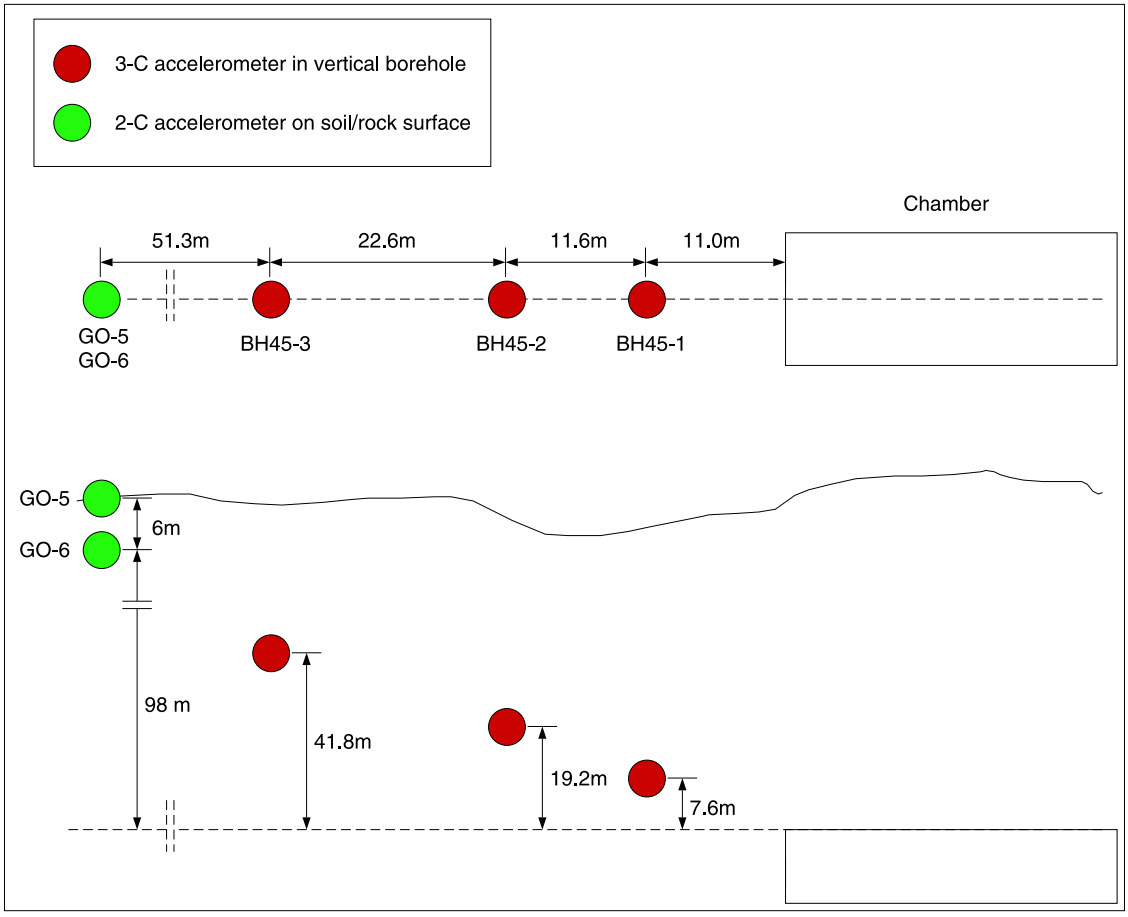

Figure 11. Accelerometer configuration relative to detonation chamber. (bottom) Location of the sensors along a cross section through the chamber, the vertical elevation of each accelerometer above the chamber, and the location of the surface above. (top) A view looking down at the chamber from above and the location of the accelerometers along a line through the chamber. Note that BH45-1,2,3 correspond to locations V1, V2, and V3 which are discussed in the text.

surface data together with the free-field data for analysis of ground motion attenuation.

[16] Raw data for two of the three explosions are shown in Figures 12 and 13, and filtered comparisons of the three explosions at two of the stations are shown in Figures 14 and 15. Note that the peak amplitude is approximately proportional to yield at common stations.

5. Numerical Simulations of Near-Field Data

[17] We performed a series of numerical simulations to model shock wave propagation from the three explosive tests that were conducted in the large Älvdalen chamber in hard rock. The tests are identified as test 3, test 4a and test 4b [*Grønsten*, 2000; *Grønsten and Krest*, 2002], and correspond to decoupled explosions 2000C348, 2001C150, and 2001C186, respectively, all in the 1000 m^3 chamber. Test 3 used 10,000 kg (10 t) of TNT, while test 4a used 2.5 t of TNT. For each of these tests, the TNT mass was divided into 10 equal masses that were emplaced well above the chamber floor on styrofoam. The axisymmetric explosive emplacement (about the long axis of the chamber) was in two rows of five TNT masses each, with row separation of 5 and 6 m between the center of each of the charge masses in a row. Test 4b had 10 t TNT equivalent, consisting of 1450 155-mm shells emplaced similarly to the earlier tests in 10 clusters of 145 shells each.

[18] As described in section 3, three-dimensional accelerometers, placed in vertical holes drilled from the surface, were used to record the near-field motions from the explosions. We generated particle velocity records by time integrating these accelerometer records. In the following sections we describe two sets of calculations: spherically symmetric finite difference calculations for an equivalent volume sphere in granite, and three-dimensional (3-D) finite difference calculations in which we model the known cavity geometry and layout of explosive in the chamber. In these calculations we model the chamber as sealed at the time of each explosion so that all explosive materials stay in the chamber. In reality, the chamber was open to the adjacent tunnel. Pressure measurements at gauges 135 m down the tunnel showed that the shock arrived at 236 s for the 2.5 t explosion, and at 222 ms for the 10 t explosion, indicating a propagation velocity of approximately 600 m/s to that point. The pressure at that point decays at a rate of 50% over 3 s after the initial

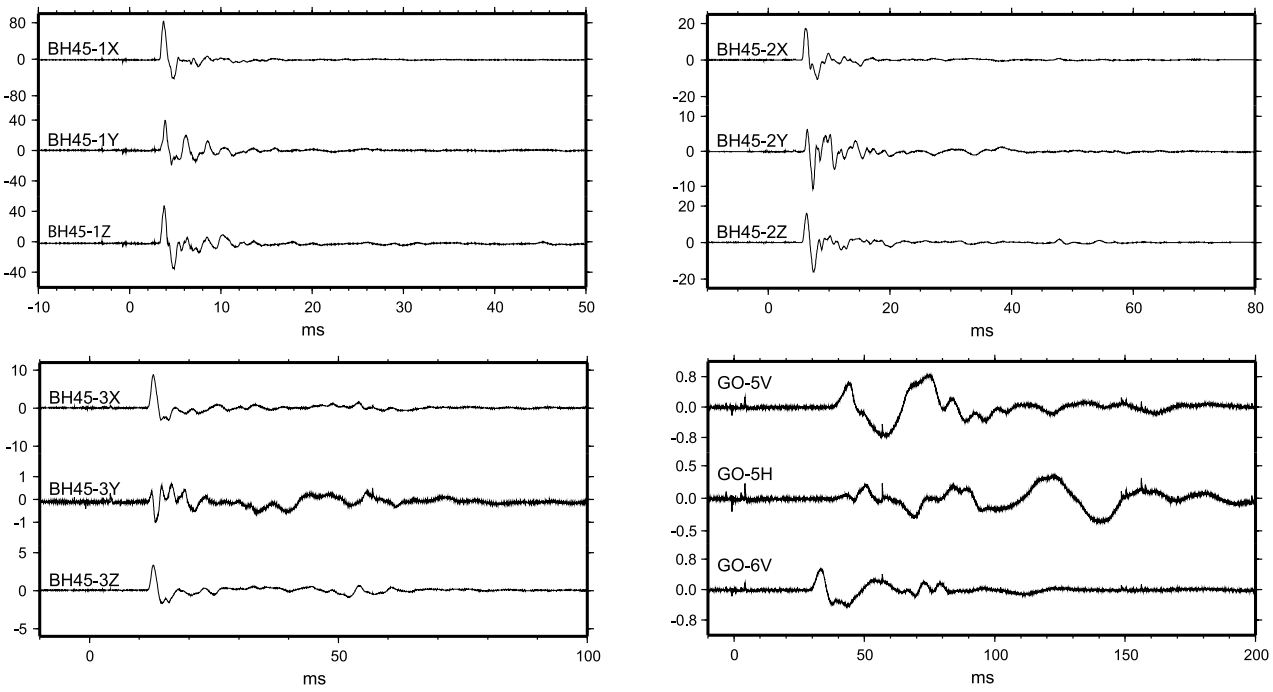

Figure 12. Near-field accelerometer recordings of the 10,000 kg TNT explosion on 13 December 2000 (2000C348). Vertical scale is in g.

shock, returning to atmospheric pressure after about 12 s. This pressure loss due to the presence of the tunnel is slow enough that the approximation of a sealed cavity for the 30 ms duration of the calculation should be adequate.

5.1. Test Geometry

[19] Test chamber dimensions are roughly 8 m in width, 4 m in height, and 30 m in length. The long axis of this chamber, the parallel direction in the original data

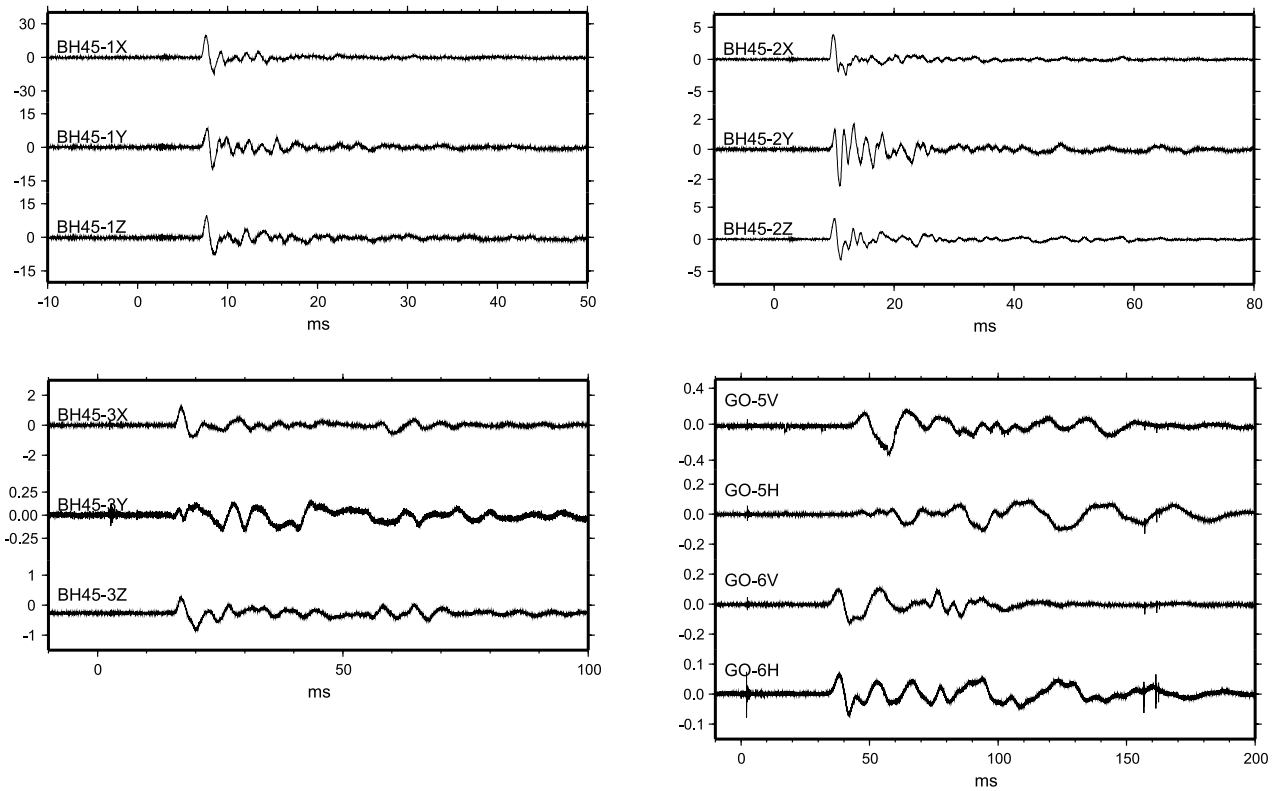

Figure 13. Near–field accelerometer recordings of the 2,500 kg TNT explosion on 30 May 2001 (2001C150). Vertical scale is in g.

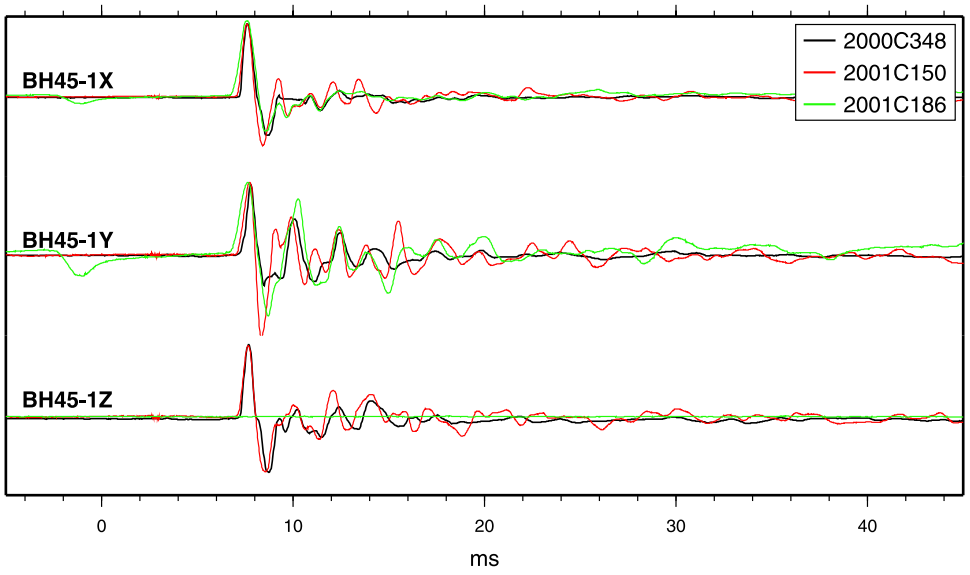

Figure 14. Comparison of the three explosions recorded at the closest borehole (BH45-1). The individual traces have been low-pass filtered and are scaled by peak value and roughly aligned on the first arrival. Note that the vertical (Z) channel for 2001C186 is defective.

reports (our x axis), is in the E-W direction, i.e., in the plane of the three grouted, vertical drill holes containing the accelerometers. This vertical x-z plane (the z axis points upward) is presumed to intersect the center of the chamber, providing a theoretical plane of symmetry since the TNT was emplaced symmetrically about the long axis of the chamber. Thus the predominant motions at the gauge locations should be in the positive x and z directions, with little motion expected in the horizontal N-S (our y) direction.

[20] The three accelerometer packages are located along a line in this vertical plane of symmetry at an angle of 45° to the vertical. This line does not go through the center of the chamber. Thus the (spherical) radial direction for our 1-D calculations is not along the axis of the three accelerometers. These three gauges, designated as V1, V2, and V3, are at slant ranges (radial distances) of 27.7, 43.1, and 74.4 m, respectively, from the center of the chamber. The coordinates of these gauges relative to the center of the chamber (xc and zc) and relative to the

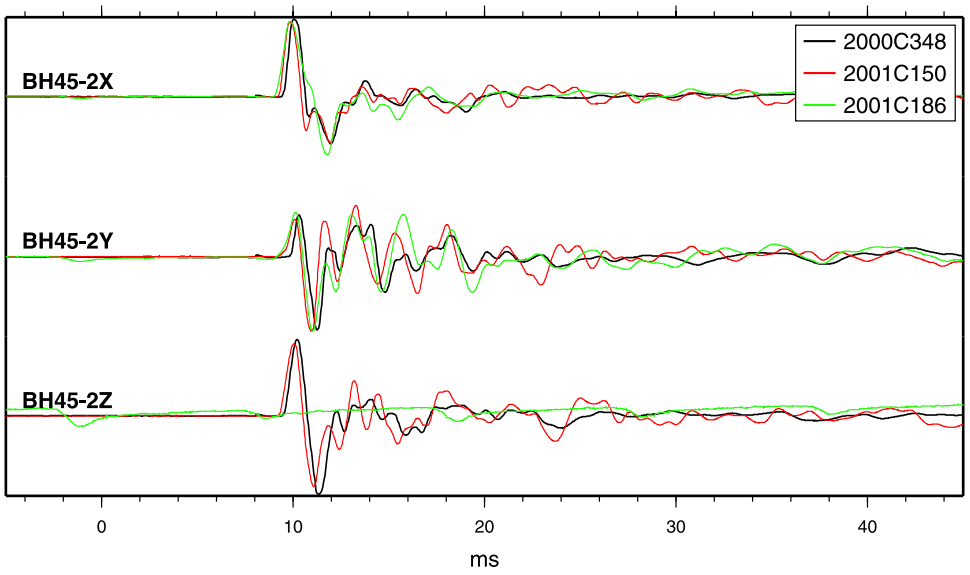

Figure 15. Same as Figure 14, but for the borehole located 23 m west of the chamber edge (BH45-2). The vertical (Z) channel for 2001C186 is also defective here.

Table 2. Coordinates of Gauges V1, V2, and V3 Relative to Center (xc, zc) and Closest Edge (xe, ze) of the Explosion Chamber for Tests 3, 4a, and 4b

Gauge	Slant Range From Center, m	xc, m	zc, m	xe, m	ze, m
V1	27.7	26.1	9.3	11.0	7.6
V2	43.1	37.7	20.9	22.6	19.2
V3	74.4	60.3	43.5	45.2	41.8

closest edge, the top for the z coordinate (xe and ze), are given in Table 2.

5.2. Data Analysis

[21] The accelerometer measurements (and integrated particle velocities) are obtained in the x, y, z, coordinate system defined above. From the raw data, we have compiled a table of results (Table 3) for the first signal at each gauge location. For many of the results, comparisons between the three explosions appear to be at least qualitatively in line with expectations. Lower peak velocities at the gauges for test 4a compared with test 3 are consistent with the more decoupled explosion. The lower peaks for test 4b, for the same mass of explosive as test 3, could be due to a lower energy content than expected in the ammunition or a slower detonation compared with the pure TNT detonated in test 3. Test 4b does give higher peaks than the more decoupled test 4a.

[22] Note that the y component of the peak particle velocity, expected to be negligible because of the plane of symmetry of the experiment, is a significant fraction of the x and z velocity components, particularly at gauges V1 and V2. This could indicate that the individual drill holes from the surface were not aligned correctly. The y velocity components from test 3 are less likely to be the result of asymmetric explosive detonation, since the direction of this y motion has changed between gauges. For test 4b, the vertical channels at V1, V2, and the transverse channel at V3, all became defective for this July 2001 explosion. Therefore these defective records are all excluded in the following discussions. The other components for test 4b are smaller than expected based on comparable yield of test 4a. This is likely due to the difference in yield efficiency of the ammunition shells used in test 4b versus the TNT used in the other tests. The regional signals were also smaller for test 4b than for test 4a.

[23] For comparison with spherically symmetric one-dimensional calculations to be discussed below (we ignore the free surface effect), we rotated the measured values of the x and z components of the particle velocities about the line from the center of the test chamber to the gauge to obtain the radial and tangential (in-plane) components, i.e., to cylindrical, rather than spherical, components. The recorded y components of the acceleration (and particle velocities) were thus treated here as a measure of unexpected large asymmetries in the results of a theoretically axisymmetric experiment.

[24] These asymmetric accelerometer measurements are not yet understood. Possible explanations include inhomogeneities in the surrounding rock, the precision of the axisymmetric gauge emplacements, and/or the symmetry of the explosion emplacements or detonations. We believe that the explosive gases venting from the chamber into the tunnel complex, while certainly an asymmetric effect, would not strongly effect first arrivals and peaks at the three accelerometers.

[25] Table 4 shows the rotated peak values of the in-plane radial (r) and tangential (t) velocity components together with the y component and the magnitude of the peak velocity vector for tests 3, 4a, and 4b. In general, the radial peak velocities are only slightly smaller than the peak velocity magnitudes. We note again that for test 4b only, gauges V1 and V2 have defective z channels and V3 has defective a y channel. Thus only t and r components are computed at V3.

[26] In the absence of the large, unexpected y components, the values of the in-plane tangential component of peak velocity may be considered a measure of the physical effect of the nonsphericity of the test chamber and explosive emplacement. Using a point source argument, this nonspherical effect would be expected to be largest for the closest gauge, V1, and smallest for the furthest gauge from

Table 3. Values of Arrival Time, Time of First Peak Velocity, Risetime, and Peak Particle Velocity Components for Tests 3, 4a, and 4b in 1000 m^3 Chamber[a]

Gauge	Arrival Time of First Signal, ms	Time of First Peak, ms	Risetime to Peak, ms	Peak of x Component, cm/s	Peak of z Component, cm/s	Peak of y Component, cm/s
			Test 3, 10 t TNT			
V1	3.4	4.1(4.3)	0.7	41.5	22	16.4
V2	5.7(6.0)	6.8	1.1	12	10.8	3.1
V3	12	13.8	1.8	9.4	3.5	−0.64
			Test 4a, 2.5 t TNT			
V1	7.2	8.0	0.8	10	4.8	4.2
V2	9.5	10.4	0.9	2.7	2.2	0.7
V3	16.1	18.1	2.0	1.5	0.4	0
			Test 4b, 10 t Ammo			
V1	7.9	9.2	1.3	21.5	defective	7.2
V2	10.1	12.1	2.0	8.1	defective	1.5
V3	16.9	19.4	2.5	5.7	2.3	defective

[a]Times for y component are shown in parentheses if different from other components.

Table 4. Values of In-Plane Radial r, In-Plane Tangential t, and y Components of Peak Particle Velocity for Tests 3, 4a, and 4b in 1000 m^3 Chambers[a]

Gauge	Peak of r Component, cm/s	Peak of t Component, cm/s	Peak of y Component, cm/s	Magnitude of Peak Velocity, cm/s
		Test 3, 10 t TNT		
V1	46.5	−7	16.4	49.8
V2	15.6	−3.9	3.1	16.4
V3	9.7	2.7	−0.64	10.1
		Test 4a, 2.5 t TNT		
V1	11	−1.2	4.2	11.8
V2	3.5	−0.7	0.7	3.6
V3	1.7	0.3	0	1.7
		Test 4b, 10 t Ammo		
V1	N/A	N/A	7.2	N/A
V2	N/A	N/A	1.5	N/A
V3	6.0	1.5	N/A	N/A

[a]Positive t velocity is counterclockwise from (upward) direction. N/A indicates defective channels involved.

the chamber, V3. In fact, Table 4 shows substantial tangential, t, components for all working gauges (10% or more of the radial component). At gauge V3 for all three tests, the tangential velocity is positive (counterclockwise from the upward direction), while at gauges V1 and V2 for tests 3 and 4a, the tangential velocity is clockwise. We do not understand this change in direction of the tangential velocity. Note, however, that the magnitude of peak in-plane tangential motion, in many cases, is quite similar to the peak y component.

5.3. Spherically Symmetric Calculations

[27] As a first step toward understanding these near-field velocity measurements, we performed spherically symmetric simulations for tests 3 and 4a and compared the results with the observations. In these finite difference calculations, the long test chamber and axisymmetric explosive configurations were approximated as a spherical mass of TNT centered in a 1000 m^3 spherical chamber of approximately 6.20 m. For test 3, the 10,000 kg (10 t) of TNT gave an outer radius of ~1.136 m for the TNT, assuming normal TNT density of 1.63 g/cm^3. For test 4a, the radius of the 2.5 t TNT sphere was calculated to be ~0.7155 m.

[28] The explosive was center detonated, with the propagation of the detonation wave through the TNT computed using the JWL equation of state. The JWL equation of state has been used to accurately describe the pressure-volume-energy behavior of the detonation products of explosive in metal acceleration applications. The equation is [*Lee et al.*, 1973]

$$P = A\left(1 - \frac{\omega}{R_1 V}\right)e^{-R_1 V} + B\left(1 - \frac{\omega}{R_2 V}\right)e^{-R_2 V} + \frac{\omega E}{V}$$

where P is pressure in Mbar, E is energy density in Mbar cm^3/cm^3 and V = (volume of detonation products)/(volume undetonated explosive). For pure TNT, the parameters are listed in Table 5.

[29] The surrounding air was modeled using an equation of state for air originally developed by the Air Force Weapons Laboratory (M. Alme, AFWL report, 22 February 1977), which has subsequently been validated through many successful simulations at SAIC. The rock surrounding the test chamber was modeled as granite.

[30] For the simulations shown here, a relatively simple model was used to describe the rock behavior. This granite model "YF-AF", from *Stevens et al.* [2003] presumed an elastic response coupled to a nonassociated radial return flow rule with a failure surface based on that measured in the laboratory on fractured granite cores from the Piledriver test site. Elastic constants used were a bulk modulus of 483 kbar, a shear modulus of 207 kbar, and a density of 2.60 g/cm^3.

[31] Figure 16 shows the velocity data and spherical calculation scaled to correspond approximately to the same yield. Using cube root scaling, increasing the yield by a factor of four leads to the same waveforms with all dimensions and the timescale increased by a factor of $4^{1/3}$. So the velocity waveform from a 2.5 t explosion recorded at a distance of gauge V1 (27.7 m) and the timescale increased by that factor should be approximately the same as the velocity waveform from the 10 t explosion at the distance of gauge V2 (43.1 m). Scaling does not work exactly because the chamber volume remains the same in the two cases. Nevertheless, it is useful for comparison. Figure 16 shows that both the data and the calculation for the 10 t case are somewhat larger than the scaled 2.5 t case, consistent with some modest increase in coupling due to nonlinear deformation from the larger explosion. The calculated waveforms at this location are larger than the observations. As discussed in section 5.4 on 3-D

Table 5. Experimental Values for Pure TNT Parameters in the JWL Equation

Parameter	Value	Unit Conversion, dyn/cm^2
A	3.712 Mbar	3.712×10^{12}
B	0.03231 Mbar	3.231×10^{10}
R1	4.15	
R2	0.95	
ω	0.30	

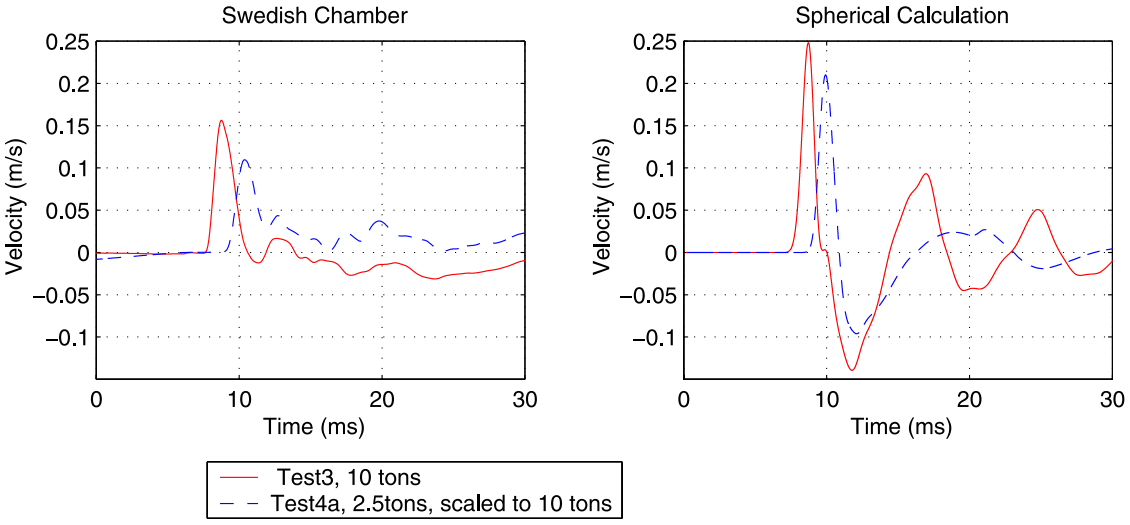

Figure 16. The 10 t chamber data and the spherical calculation at gauge V2 (red lines) and the 2.5 t data and calculation at gauge V1 (blue lines), scaled to 10 t (by increasing timescale by $4^{1/3}$) which is approximately equivalent to recording at V2. Coupling predicted from the spherical calculation is larger than the data at this location.

calculations, this is due to the location of the gauges off the long end of the chamber.

[32] Figure 17 shows a comparison between the "observed" decoupling factors for the Swedish explosions and decoupling factors for a series of 28 calculations of chemical explosions with yields between 0.1 and 100 t. "Observed" is in quotes because we do not have data from a tamped explosion for comparison. Instead, we use

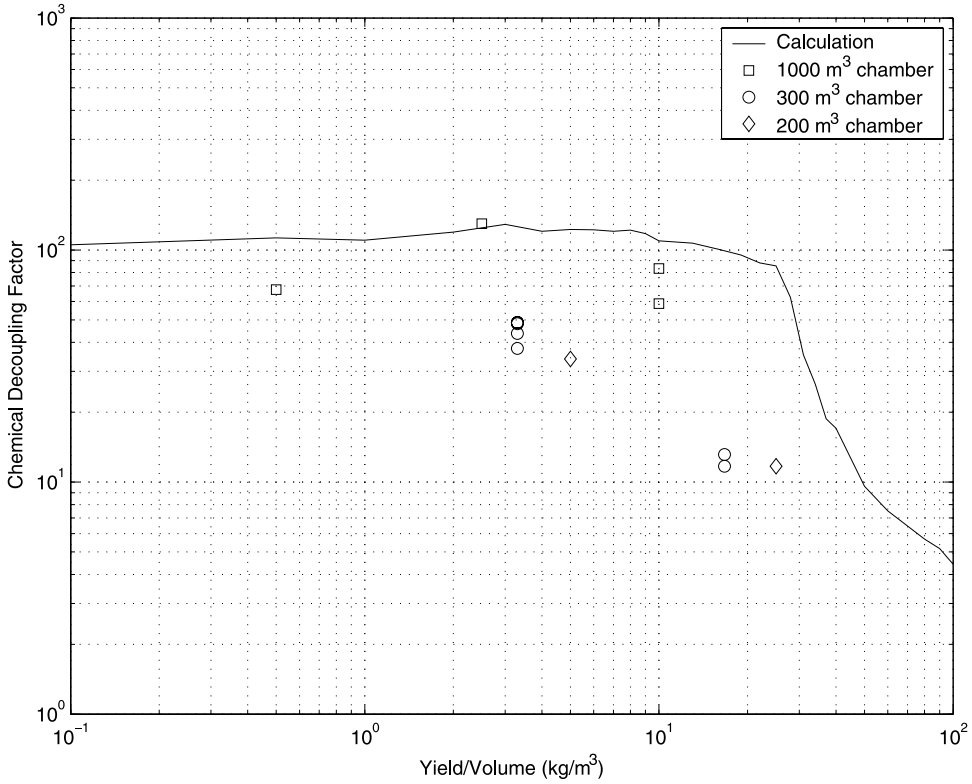

Figure 17. Observed and predicted decoupling factor for Swedish chamber explosions. Calculations were for a chemical explosion in a 6.2 m spherical cavity in hard (nonweakening) granite. Since there is no equivalent tamped explosion, the observed decoupling factor is normalized using an empirical magnitude/yield relation as discussed in the text. The horizontal axis corresponds approximately to the overdrive factor above full decoupling.

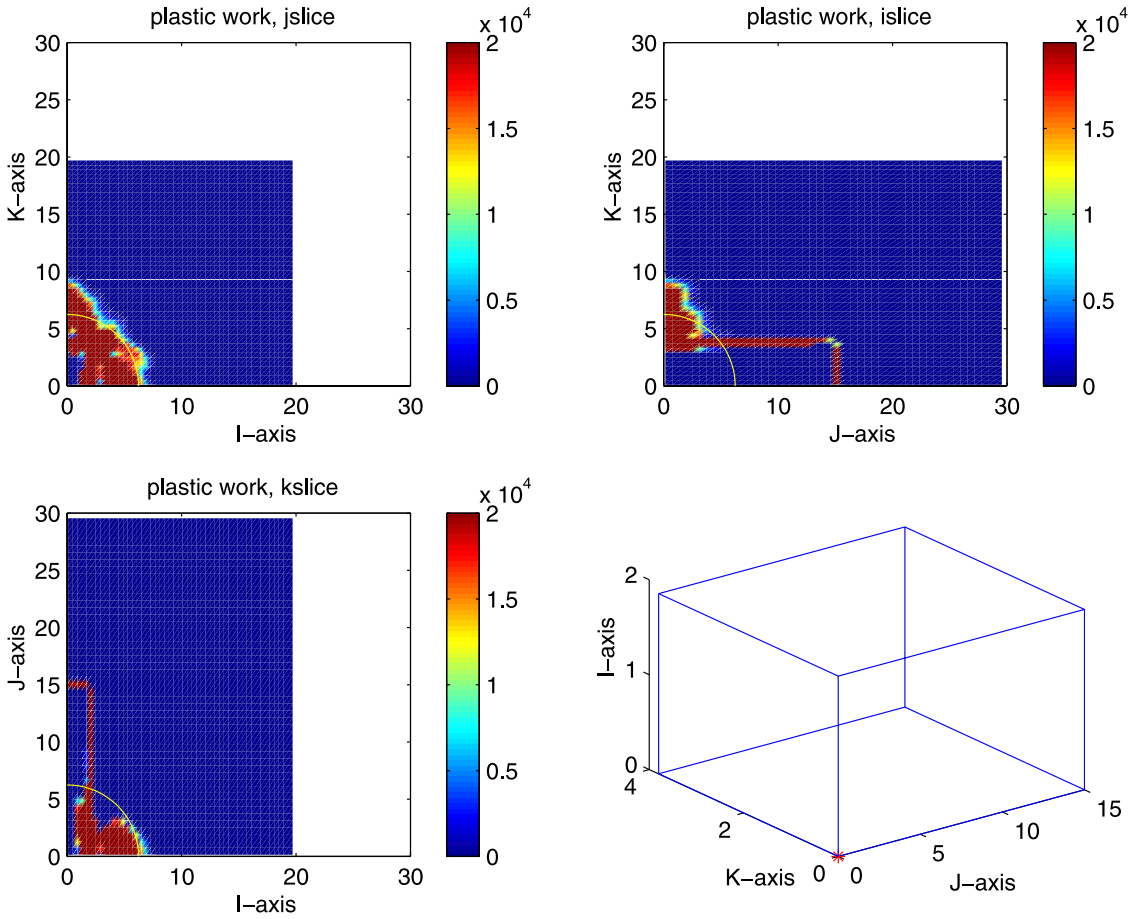

Figure 18. Regions of nonlinear deformation for the 2.5 t chamber calculation. The nonlinear deformation around each of the three axes is shown. The yellow line is the region of nonlinear deformation for an equivalent volume sphere.

the magnitude/yield relation from *Murphy* [1996] m_b = 4.45 + 0.75logW, where W is yield in kilotons to estimate the magnitude of a tamped explosion. For a yield of 10 t, this gives an estimated m_b 2.95. Two of the events have reliable magnitudes listed in the NORSAR Regional Event Bulletins [*Ringdal and Kvaerna*, 1989]: 2000348 with m_b 1.22 and 2001186 with m_b 1.00. A third event, 2002164, also has a NORSAR magnitude but examination of the records shows that it was mislocated and included a misassociated arrival. A more recent 10 t event on 2005166 had an m_b of 0.99. Using the magnitudes of events of 2000348 and 2001186, we estimate decoupling factors of 54 and 90, respectively. We then use the average of these decoupling factors to normalize all of the data.

[33] As noted before, the larger chamber appears to decouple better than the smaller chambers for the same charge density. Figure 17 shows that the explosions remain almost fully decoupled until the charge/volume is approximately equal to 10, after which increases in yield cause a rapid decrease in decoupling. The calculation also shows this effect of nearly constant decoupling followed by a rapid decline. In the calculation the decline occurs at a higher charge/volume, most likely because the Swedish cavities are not spherical, which increases coupling. We investigate this further with 3-D calculations in section 5.4.

5.4. Three-Dimensional Calculations

[34] In order to increase our understanding of the Swedish chamber explosions, several three-dimensional finite difference calculations were performed using the "Stellar" code. Stellar is a second-order accurate Eulerian two- and three-dimensional stress wave propagation code with the same constitutive models that were used for the spherically symmetric calculations. The chamber was modeled as an air-filled chamber with dimensions 4.8 m high (x axis), 30 m long (y axis), and 7.2 m wide (z axis). The near-field results are sensitive to the layout of the explosive in the chamber, so several layouts were used in the simulations. All calculations were performed in a 1/8 space, taking advantage of symmetry across the three planes through the center of the rectangular chamber. In this first calculation, the finite difference grid was 20 m × 30 m × 20 m in size, with 100 × 100 × 100 grid blocks. The chamber is 2.4 m × 15 m × 3.6 m. The explosive was placed in a flat layer along the x = 0 plane, with a dimension of 0.2 m × 2.7 m × 0.8 m, with a total energy

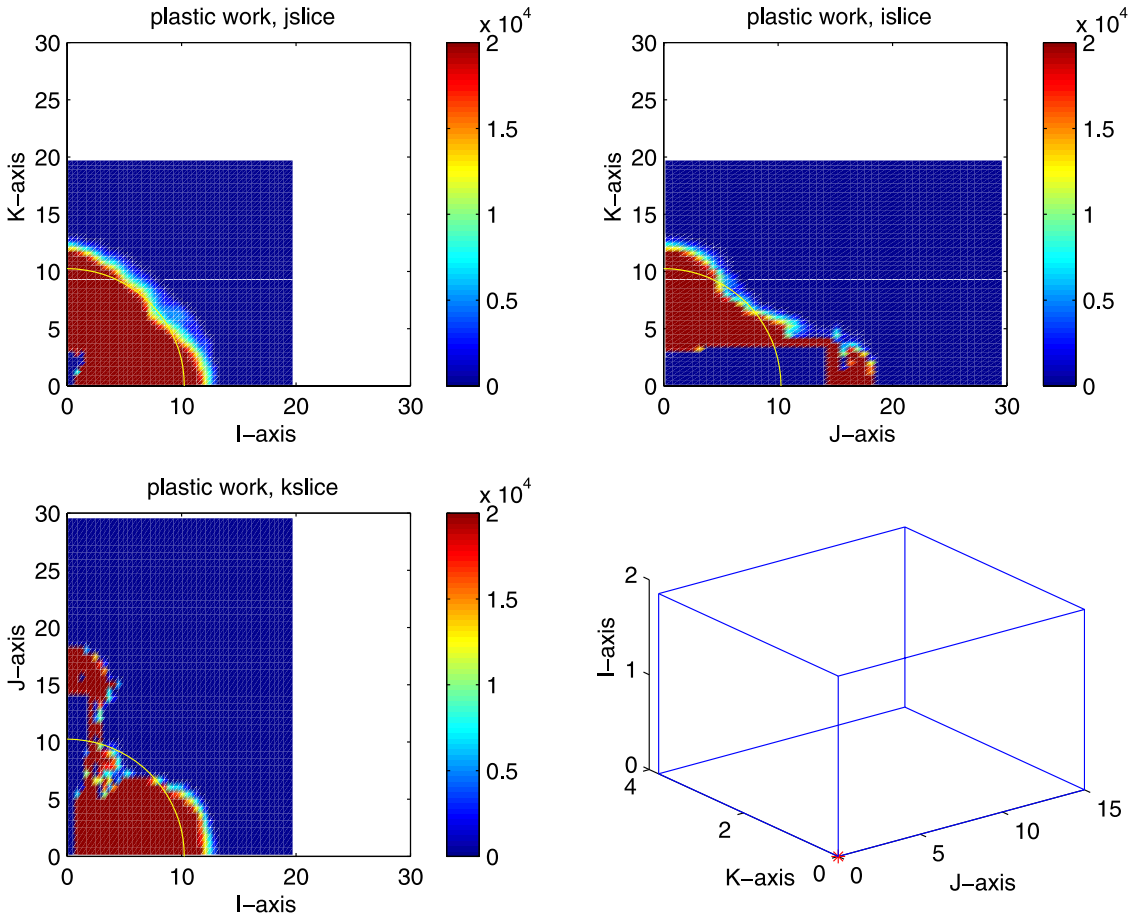

Figure 19. Regions of nonlinear deformation for the 10 t chamber calculation. The nonlinear deformation around each of the three axes is shown. The yellow line is the region of nonlinear deformation for an equivalent volume sphere.

of 1.25 t. Note that because of symmetry, all linear dimensions are effectively multiplied by two and volumes by eight, so this is equivalent to a 10 t explosion in the chamber described earlier. A second calculation was performed with the same geometry, except that the explosive was reduced to an area of 0.2 m × 2.7 m × 0.2 m, corresponding to a total energy (including symmetric regions) of 2.5 t. Figures 18 and 19 show a comparison of the regions of nonlinear deformation for these two calculations.

[35] A third set of calculations was performed with an explosive distribution more consistent with the actual layout of explosives, which was set out in a series of small pads dispersed over a larger part of the chamber. We model this in the simulation as two pads which by symmetry corresponds to 8 pads each of twice the thickness used in the calculation. The result is two strong initial pulses, and a more complicated state within the chamber, but a somewhat reduced effect on the chamber wall.

[36] Figure 20 shows that calculated waveforms at the locations of recording stations V1 and V2, together with the horizontal and vertical components of the recorded waveforms at the same locations. As with the spherical calculations, the chamber reverberations are stronger than the observations; however, the peak amplitudes and general shape and duration of the waveforms are reproduced fairly well. As noted above, there is a strong radiation pattern to the waveforms, with stronger amplitudes above and below the chamber and reduced amplitudes along the long axis of the chamber near the recording points V1 and V2.

6. Conclusions

[37] We collected and analyzed data from 15 partially decoupled chemical explosions conducted in rectangular chambers at Älvdalen, Sweden. This data set covers a range of yields overdriven beyond full decoupling according to the Latter criterion by factors of up to 25. We find that decoupling remains approximately complete for yields less than 10 times the Latter decoupling criterion. At higher yields coupling increases rapidly, increasing by an order of magnitude for a factor of 2 increase in yield/volume. Even the fully decoupled 2500 kg explosion is detectable at NORSAR at a distance of 140 km. Although waveforms could not be seen in individual traces, the 500 kg explosion was detectable using waveform correlation.

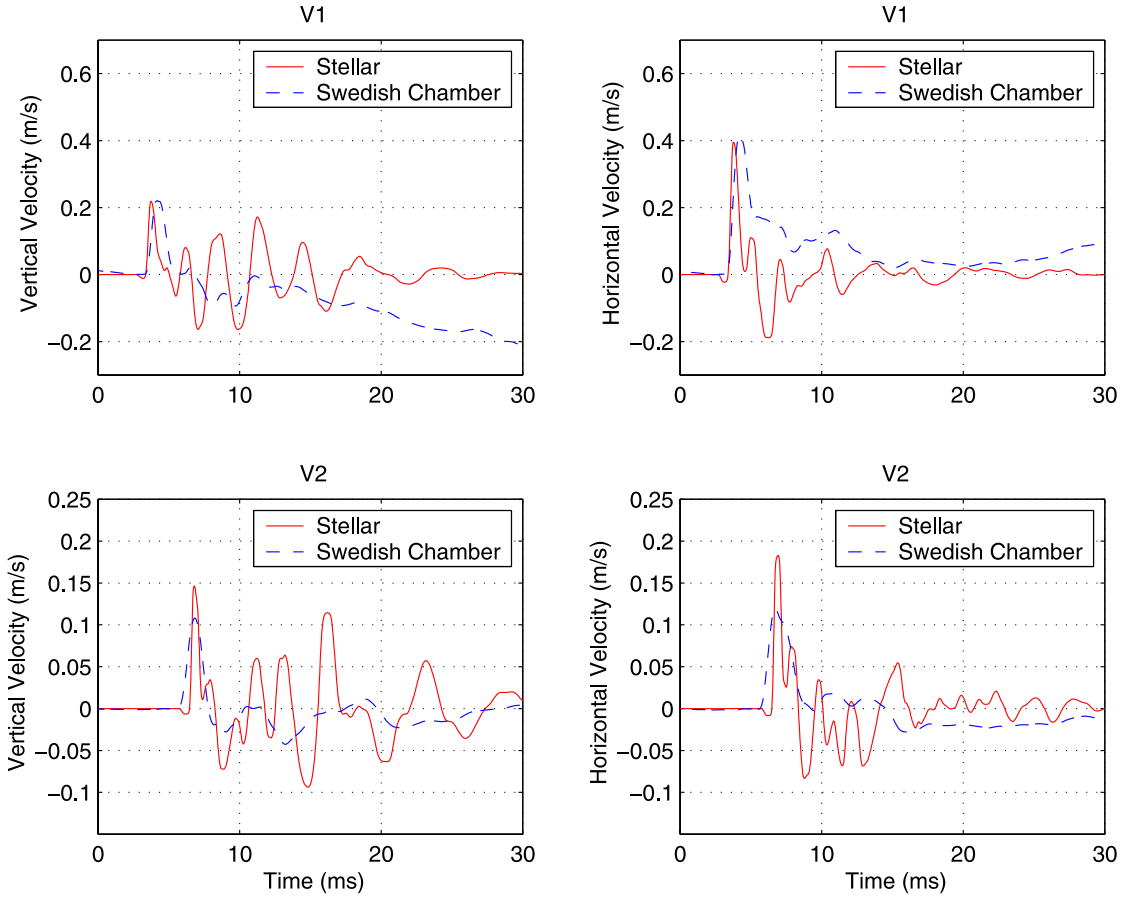

Figure 20. Data and calculated waveforms at stations V1 and V2.

[38] Three-dimensional nonlinear calculations of the chamber explosions show strong nonlinearity at the points closest to the explosion. Calculations show stronger near-field waveforms in this direction, with reduced amplitudes off the ends of the chamber where the measurements were made. Calculations are found to be generally consistent with the limited observational data set except that cavity reverberations are observed to die out more quickly than predicted by the calculations.

[39] **Acknowledgments.** The explosions discussed in this paper were conducted in a cooperative effort between the Norwegian Defense Building and Infrastructure Agency (Forsvarsbygg), Defense Science and Technology Agency (DSTA) of Singapore and the Swedish Defense Research Agency. The lead agency of the large-scale tests, DSTA, and the other participants, kindly provided the data. We thank them for their support and for the use of their data. This study was supported by contract DTRA01-01-C-0069, initially administered by the Defense Threat Reduction Agency and later transferred to the Air Force Research Laboratory.

References

Forsén, R., H. Hansson, and A. Carlberg (1997), Large scale test on mitigation effects of water in the KLOTZ club installation in Älvdalen, *Rep. FOA-R-97-00470-311*, Swed. Def. Res. Estab. (FOA), Linkoping, March.

Grønsten, G. A. (2000), The Älvdalen large scale tests, data report from the Norwegian measurements, *Fortifikatorisk notat 286/01*, Forsvarets Bygningstjeneste, Oslo, Norway.

Grønsten, G. A., and O. Krest (2002), The Älvdalen large scale tests, data report from the Norwegian measurements, *Fortifikatorisk notat 297/01*, Forsvarets Bygningstjeneste, Oslo, Norway, 2001.

Hansson, H., and R. Forsén (1997), Mitigation effects of water on ground shock: Large scale testing in Älvdalen, *Rep. FOA-R-97-00510-311-SE*, Swed. Def. Res. Estab. (FOA), Linkoping, May.

Herbst, R. F., G. C. Werth, and D. L. Springer (1961), Use of large cavities to reduce seismic waves from underground explosions, *J. Geophys. Res.*, *66*, 959.

Lee, E., M. Finger, and W. Collins (1973), JWL equation of state coefficients for high explosives, *Rep. UCID-16189*, Lawrence Livermore Laboratory, Livermore, Calif., 16 Jan.

Murphy, J. R. (1996), Types of seismic events and their source descriptions, in *Monitoring a Comprehensive Test Ban Treaty, Proceedings of the NATO Advanced Study Institute*, pp. 225–245, Springer, New York.

Murphy, J. R., I. O. Kitov, N. Rimer, V. V. Adushkin, and B. W. Barker (1997), Seismic characteristics of cavity decoupled explosions in limestone: An analysis of Soviet high explosive test data, *J. Geophys. Res.*, *102*, 27,393–27,405.

Ringdal, F., and T. Kvaerna (1989), A multi-channel processing approach to real time network detection, phase association, and threshold monitoring, *Bull. Seismol. Soc. Am.*, *79*, 1927–1940.

Stevens, J. L., J. R. Murphy, and N. Rimer (1991), Seismic source characteristics of cavity decoupled explosions in salt and tuff, *Bull. Seismol. Soc. Am.*, *81*, 1272–1291.

Stevens, J. L., N. Rimer, H. Xu, G. E. Baker, and S. M. Day (2003), Near field and regional modeling of explosions at the Degelen Test Site, SAIC final report to DTRA, *Rep. SAIC-02/2050*, SAIC, San Diego, Calif., Jan.

Thomson, D. J. (1982), Spectrum estimation and harmonic analysis, *Proc. IEEE*, *70*(9), 1055–1096.

Vretblad, B. (1991), Klotz club tests 1986–1989, *Rep. C1:91*, Fortifikationsförvaltningen, Forskningsbyrån, Eskilstuna, Sweden.

Wu, C., Y. Lu, W. K. Kim, Y. Zhou, and C. C. Seah (2003), Characterization of underground blast-induced ground motions from large-scale field tests, *Shock Waves*, *13*, 237–252.

S. Gibbons, T. Kvaerna, C. Lindholm, and F. Ringdal, NORSAR, Post Box 53, NO-2027 Kjeller, Norway.

J. R. Murphy, N. Rimer, J. L. Stevens, and H. Xu, Science Applications International Corporation, 10260 Campus Point Drive, San Diego, CA 92121, USA. (jeffry.l.stevens@saic.com)